Impact-abrasive and abrasive wear behavior of low carbon steels with a range of hardness-toughness properties

Gourab Saha, Kati Valtonen, Ari Saastamoinen, Pasi Peura, Veli-Tapani Kuokkala

Tampere University, Faculty of Engineering and Natural Sciences, Tampere Wear Center, Tampere, Finland

Abstract

This work investigates steels for mining wear applications involving abrasive and impact-abrasive conditions. The study comprises four low carbon steels with a range of hardness-toughness combinations: a commercial grade martensitic steel, the same steel heat treated to lower bainite, a commercial TRIP steel (tensile strength grade 700 MPa), and a quenching-partitioning (QP) steel. The steels were subjected to crushing pin-on-disc (CPOD) and slurry-pot wear tests, offering reasonably high-stress abrasive and impact-abrasive conditions, respectively. The results showed that the best performer in both studied wear conditions is the martensitic steel due to its higher initial hardness. Nevertheless, the performance benefit of this steel was of lesser magnitude in the slurry-pot than in the CPOD tests. On the other hand, the TRIP steel showed poor ranking in the CPOD tests but outperformed the QP and lower bainite steels in the slurry-pot tests. Detailed surface and subsurface wear damage investigations were conducted to study the wear responses of the microstructural constituents of the steels to explain their wear behavior in different wear conditions.

Keywords: Impact-abrasive wear; Mining and mineral processing; Steels; Retained austenite; Transformation induced plasticity (TRIP); Wear testing.

1. Introduction

For decades, researchers have put significant effort in engineering the hardness and toughness of steels by modifying their microstructures in order to improve the wear resistance. The chronological development of steels from ferritic and ferrite with pearlitic colonies with increasing carbon content, followed by bainitic microstructures, has shown improved strength and wear resistance in sliding wear conditions [1–3]. The works of Clayton and Devanathan [1] and Shipway et al. [2] strongly suggest that lower bainite offers better wear resistance than pearlitic and upper bainitic microstructures, due to the refined tough matrix and the absence of brittle martensite. Moreover, the higher initial hardness and aggregation of very fine cementite and retained austenite inside the bainitic matrix seem to provide

appreciable wear resistance [3]. Despite early reports [1–4], the wear behavior of lower bainite is still not clear in heavy mining wear conditions, because most of those studies were performed using low-stress abrasion tests [5,6], which are known to correlate poorly with the real mining wear conditions.

In general, martensitic steels show good wear resistance due to their initial hardness [7]. Nonetheless, the work of Valtonen et al. [8] demonstrated that work hardening increases the wear resistance of martensitic steels in high stress wear conditions. An additional feature of martensitic steels is that pure abrasion can sometimes produce a brittle white layer on the surface [9], while the impact-abrasive wear conditions may lead to the formation of adiabatic shear bands (ASB) [8] along with the surface white layers, contributing to the material removal [10]. Both of these microstructural features share a similar nanostructured untempered martensitic structure with significantly increased hardness [8]. A sufficiently high strain rate causes localized deformation producing ASBs [11], which facilitates damage accumulation and fragmentation [12,13] during the wear process. The earlier studies lack a systematic comparison of the wear behavior of martensitic steels to their lower bainitic counterparts of the same alloy composition at different wear conditions relevant to mining.

If the application demands toughness along with hardness, then martensite combined with a retained austenitic microstructure, such as in TRIP assisted and quenching-partitioning (QP) steels, is a potential choice. During impacts, the strength of martensite provides resistance against particle penetration, while the finely distributed inter-lath retained austenite absorbs the strain energy and transforms to martensite, popularly known as the transformation induced plasticity or the TRIP effect [14]. The TRIP steels' microstructure consists of soft primary ferrite and retained austenite along with hard phases such as martensite and bainite in varying amounts. The transformation behavior depends on several factors, including a critical stress level [15], temperature [16], strain rate [17], and tensile loading, as the retained austenite transforms to martensite more easily in tensile than compressive loading [18]. The morphology of the metastable austenite is an equally important factor that governs the transformation behavior [19,20]. The TRIP steels are used for example in the automotive industry due to their excellent work hardening and forming capacity. Nevertheless, literature suggests that a methodical approach to exploit the superior strength-ductility properties of the TRIP steels is absent for manufacturing of mining components.

In the recent past, quenching-partitioning steel (QP) with superior strength-toughness properties compared to quenched-tempered (QT) martensite was developed by Speer et al. [14,21]. In the QP processing, the steels are austenitized, quenched between the martensite start (M_s) and finish (M_f) temperatures, and isothermally held at some higher temperature so that carbon atoms can diffuse from

the supersaturated martensite to austenite, resulting in a microstructure consisting of martensite and partly stabilized austenite. The design of the microstructure necessitates a careful use of Si, Al or P to retard the cementite precipitation and decomposition of the retained austenite [14,22]. However, the wear response of the QP steels at different wear conditions has not been much explored. Hu et al. [19] heat treated a 0.95 %C steel to obtain nanostructured bainitic and QP martensitic microstructures with a reasonable amount of retained austenite. The steels were studied using a stirring wear test that mimics the cement mixer working conditions. In the wear tests, the QP treated steel exhibited better wear performance than its nanostructured counterpart. Further studies showed that the morphology of the retained austenite in the QP steel was film shaped, in contrast to the blocky morphology of retained austenite in the nanobainite, which resulted in a higher wear loss [19]. A similar improved wear resistance was reported by Wang et al. [23] for a 0.20 %C QP steel under impact-abrasive wear conditions, attributed to the TRIP effect of the retained austenite. In contrast, Haiko et al. [24] recently reported a lower wear resistance of a QP steel compared with a quenched tempered steel (~0.3 %C) in the impact-abrasive impeller-tumbler tests. However, the QP steel had a clearly lower initial hardness. As an explanation, Haiko et al. [24] suggested an adverse TRIP effect where the matrix failed to accommodate the transformation stresses, facilitating the subsurface crack formation and propagation.

The selection of steels for a particular application depends on how closely the laboratory experimental set-up captures the dynamics of the true tribo-environment [8,25]. For mining and mineral processing applications, the test method needs to simulate various wear mechanisms occurring in the field [9,10], including impact actions [28,37,38] and/or scratching by the penetrating sharp edges of the particles [26,39–43] A number of non-standard test methods that provide promising correlation with the field data have been developed in recent years, such as the crushing pin-on-disc (CPOD) [44], impeller-tumbler [45], and high-speed slurry-pot tests [46]. The CPOD test method provides efficient reproduction of the ore crushing and gouging actions. On the other hand, impeller-tumbler [27,45] and high-speed slurry-pot offer an impact-abrasive wear mechanism [8,9,47], prevalent in impact crushers and mineral comminution applications. Of these two methods, the high speed slurry-pot tests offer a higher wear rate compared to the impeller-tumbler tests [8]. In addition to the test method, the selected abrasive has a marked effect on the wear environment and the test results [9,49]. Quartzite with high hardness and quite homogenous composition is typically used in abrasive wear tests. However, during the high stress abrasive or impact-abrasive tests it comminutes pretty fast, and especially the finest flakes embed into the steel surfaces and affect the wear rates [49]. Also, in certain wear environments granite(s) may produce lower wear rates due to higher attrition rate compared to quartzite. Valtonen et

al. [9] also demonstrated that granite as an abrasive differentiates the steel grades better in abrasive wear tests than quartzite.

In this study, a systematic approach was followed in the selection of the low carbon steels based on their hardness and toughness properties. A commercial high hardness martensitic steel was studied and also re-heat treated to gain a fully lower bainitic microstructure with improved toughness properties at the expense of the hardness of its 'parent' martensitic steel. Neither of these microstructures contains retained austenite to provide the TRIP effect during impact conditions. Therefore, a commercial TRIP steel and a QP steel were also studied to generate an understanding on the behavior of the steels' microconstituents in both abrasive and impact-abrasive wear conditions. The crushing pin-on-disc (CPOD) and high-speed slurry-pot tests were employed as the application relevant wear tests for both wear conditions.

2. Materials and methods

2.1 Materials

This study employs four types of steels, denoted as martensite, lower bainite, TRIP, and QP (quenching-partitioning) steels. The chemical compositions and the corresponding bulk hardness of the steels are listed in Table 1.

Table 1: Chemical composition (wt %) and bulk hardness of the steels determined using a 5 kg load. S.E represents the standard error corresponding to the bulk hardness of the steels.

Steels	C	Si	Al	Mn	Cr	Mo	Cu	Ni	Nb	HV5	S.E
Martensite	0.30	0.80	-	1.70	1.50	0.50	-	1.0	-	497	4.01
Lower bainite	0.30	0.80	-	1.70	1.50	0.50	-	1.0	-	397	2.52
TRIP	0.19	0.42	1.25	1.64	-	0.04		-	-	198	2.97
QP steel	0.19	0.38	1.96	1.99	0.11	0.35	.02	0.02	.03	268	1.93

The martensitic steel is a commercial grade high-strength 500 HB wear resistant steel, obtained using the direct-quenching production technology. The XRD analysis of the steel reveals a martensitic microstructure with less than 1 % retained austenite. JMatPro® [50] simulation software was used to design the heat treatment of the lower bainite using the previous martensitic steel. The simulation suggested an austenitization temperature of 810 °C and 275 °C as the martensitic start temperature (M_s). The steel was austenitized for 4 minutes at 850 °C and quenched in a salt-bath preheated to 325 °C,

resulting in a cooling rate up to 100 °C/s. The steel was held isothermally at 325 °C for 5 hours and 30 minutes, followed by air cooling to room temperature, yielding a fully lower bainitic microstructure. The commercial TRIP steel was cold rolled to 1.2 mm, followed by partial austenitization by intercritical heat treatment for 30 s. The QP steel was vacuum cast as 2 kg billets of size 40×40×180 mm^3 and subsequently homogenized at 1200 °C for 30 minutes. The specimens were then hot rolled above the recrystallization temperature to 3 mm sheets, followed by a cold rolling operation to further reduce the thickness of the sheets to 1.3 mm. In a previous research [51], the same steel was annealed intercritically between the A_1 and A_3 temperatures to improve its formability. In the current case, the steel required higher strength to be able to combat severe mining wear. Because of this, considering 0.3 %C in the austenite, the JMatPro® [50] simulation recommended an austenitization temperature of 935 °C and the corresponding M_s and M_f temperatures of 350 °C and 235 °C, respectively. Based on the simulation results, the steel was finally austenitized at 935 °C for 4 minutes and subsequently quenched at a cooling rate up to 100 °C/s in a salt-bath at 270 °C, where it was held isothermally for 20 s. The specimens were then directly transferred to another salt-bath heated to 350 °C, where the partitioning treatment was performed for 200 s, followed by air cooling to room temperature.

2.2 Crushing pin-on-disc abrasive wear testing

The crushing pin-on-disc (CPOD, Fig. 1a) [44] test method is a three-body abrasive wear test based on the principle of the ordinary pin-on-disc test. In the CPOD test, however, the equipment allows 500 g of gravel of size 2-10 mm in each test cycle, offering high-stress abrasive wear conditions. The set-up consists of a cylindrical pin specimen (h-35 mm, ∅-36 mm), inserted vertically and tightened with set screws into a sample holder. Approximately 2-5 mm of the sample remains outside the sample holder so that during testing only the sample area contacts the abrasives. The sample pin is then cyclically pressed at a normal force of 240 N against a rotating gravel bed placed on a disc made for example of the structural S355 steel (216 HV, load 5 kg), as done in this study. The relatively soft steel disc embeds gravel particles during the test process, leading to an increase in the sliding abrasive wear [44]. The TRIP and QP steel samples had a thickness of less than 2 mm, and thus the samples were glued to a martensitic steel pin and cured overnight. During the disc rotation, the sample pin meets the gravel bed for 5 s, after which the bed rotates freely for 2.5 s without any contact with the pin, resulting in a total 20 min contact time for a 30 min test cycle. When the sample is in contact with the gravel bed, it forms a pile-up of gravel in front of it. The disc rotation speed is controlled manually in a range of 28-30 rpm, so that the sample pin always lands on top of the abrasive pile. Kuru granite was used as the gravel in the tests with a size distribution of 50 g 2–4 mm, 250 g 4–6.3 mm, 150 g 6.3–8 mm,

and 50 g 8–10 mm for each test cycle. A 15 minutes run-in was performed prior to each 30 min test cycle with 500 g of 4–6.3 mm granite to achieve the steady-state wear regime. In contrast to the previously reported tests [48], the 30 min test cycles were run uninterrupted. The amount of wear is quantified as the mass difference of the sample before and after the wear test. However, in this work the mass of the sample determined after the 15 minutes run-in test was considered as the initial mass of the sample, while the final mass was recorded after 30 minutes of uninterrupted testing. The average mass loss of three tests of each sample type is reported as the mass loss of the material.

2.3 High-speed slurry-pot wear testing

The high-speed slurry-pot test equipment (Fig. 1b) was utilized in this study as it reportedly offers an impact-abrasive wear environment [46,47]. The pin mill type sample arrangement comprises a rotating shaft containing sample fixtures at different levels. The detailed design and the test procedure of the slurry-pot device are described in [46,47]. In the present study, the slurry-pot test apparatus was filled with 9 kg of dry 8–10 mm Kuru granite gravel with 10 l of water. The specimens were square shaped ($40\times40\times6$ mm^3) and fixed at 90^o angle to the rotating shaft to achieve severe wear conditions. The shaft was rotated at 2000 rpm entailing an outer edge tangential speed of 20 m/s. The test program for the four steels was designed following the sample rotation method described in [46]. The test duration was 20 min, comprising four 5 min cycles, after each of which the sample positions were changed and the slurry was replaced. According to the sample rotation scheme, the sample positioned in the highest slot was placed to the lowest level for the next five minutes of testing, and all the other samples were elevated by one slot. At the end of each 5 min cycle, the samples were cleaned ultrasonically, dried and weighed to determine the mass loss and converted to the volume loss using density calculations.

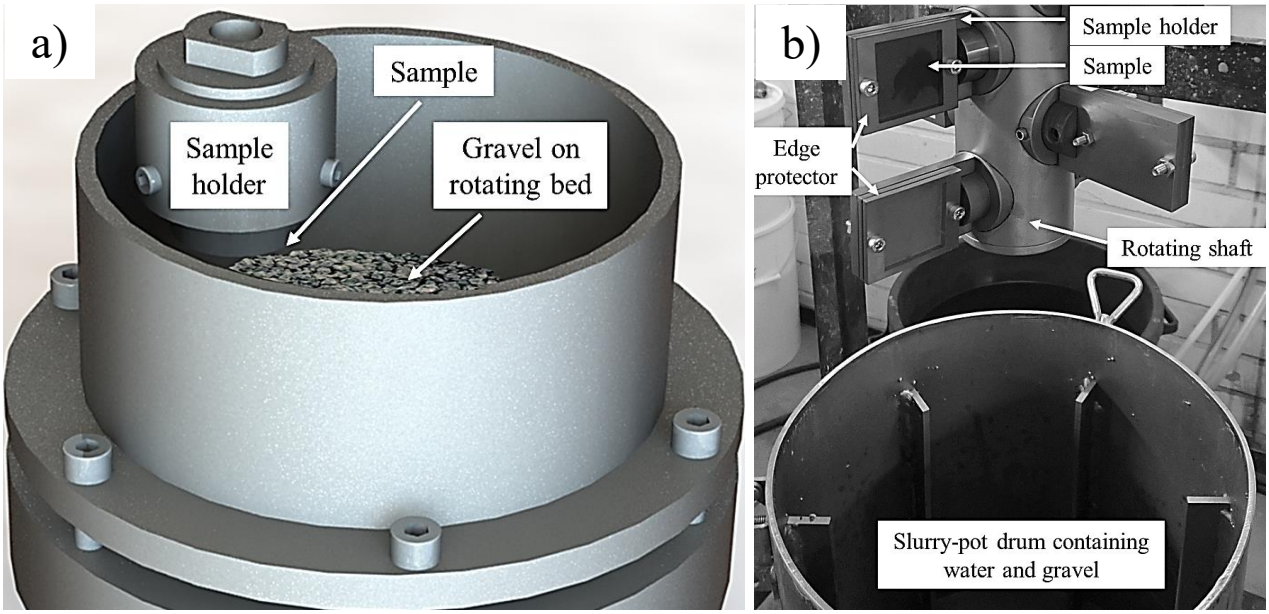

Fig. 1. Wear test equipment; a) the crushing pin-on-disc and b) the high-speed slurry-pot.

2.4 Comparison of the wear rates from different test types

Since the slurry-pot and CPOD are clearly different kinds of wear testing methods with different wear areas, an attempt was made to normalize the wear rates. The measured weight losses were converted to volume losses per unit time and unit wear area so as to enable a (reasonable) comparison of the test results. If the wear rate in both types of wear tests is $WR_{mm/h}$, Δm is the mass loss of the sample, A the wear area, t the contact time, and ρ the density of the steel, we can write [7];

$$WR_{mm/h} = \frac{\Delta m}{t.A.\rho} = \frac{\Delta v}{t.A} \qquad \text{(Eq. 1)}$$

where Δv is the volume loss. Consequently, the wear rates of the steels are expressed in the units of mm/h [7]. For the present calculations, the wear test areas for the slurry-pot and CPOD test samples were measured geometrically, the contact time was 20 min for both types of tests, and the steel density was taken as 7850 kg/m^3.

2.5 Characterization techniques

Alicona InfiniteFocus G5 optical 3D profilometer was used to investigate the wear surface features. The scan was set to vertical and horizontal resolutions of less than 250 nm and 3 μm, respectively, using the 20x objective lens. The surface roughness values were evaluated and compared with the wear rates of the steels. Moreover, the impact craters formed during the slurry-pot experiments were characterized by evaluating the crater depths (d) and the radii of contacts (a). The degree of penetration

(D_p), as originally proposed by Hokkirigawa and Kato [52], is expressed as;

$$D_p = d/a \qquad \text{(Eq. 2)}$$

As an example, an impact profile of the QP steel wear surface is presented in Fig. 2, obtained using the Alicona 3D optical profilometer. Similar impact profile characterization work is described in more details elsewhere [28]. For each slurry-pot tested steel, a minimum of five impact craters were chosen for this analysis. Additional care was taken to exclude overlapping craters and/or ridges where the zero-reference line could not be reliably determined.

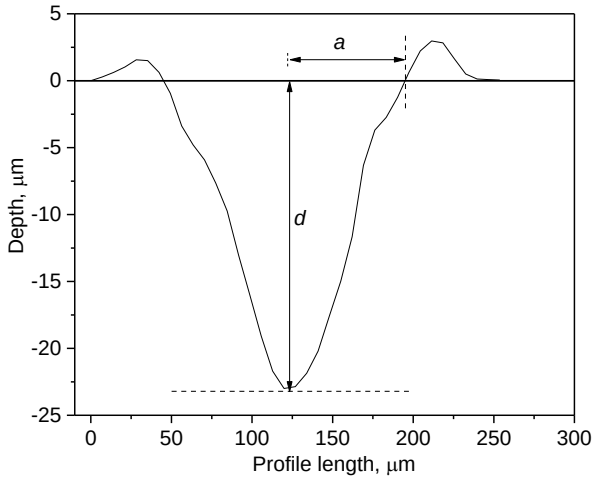

Fig. 2. An example of slurry-pot tested QP steel wear surface impact crater profile, depth (d) = 23 μm and contact radius (a) = 77.52 μm, corresponding to D_p = ~ 0.30.

D_p is an important parameter for the identification of the severity of wear in the sliding conditions. Hokkirigawa and Kato [52] suggested a transition of the wear mechanism from microploughing to microcutting through wedge formation with an increase in the groove depth. By considering the impact marks approximately as grooves of shorter lengths and wider breadths, the same approach can be applied to understand the wear modes involved in the slurry-pot test results.

The wear surface features were characterized using Jeol JSM-IT500 InTouchScope™ Scanning Electron Microscope (SEM). The microstructures and the corresponding subsurface damages were characterized by Zeiss ULTRA plus high-resolution FEGSEM. The sample cross-sections were mechanically polished, etched with 4 % nital solution, ultrasonically cleaned in ethanol, dried and stored overnight in vacuum before the SEM studies. In contrast, the samples corresponding to the damaged wear surfaces were only cleaned ultrasonically in ethanol and dried before characterization. The Vickers macrohardness was measured using Struers Duramin-A300 with a 5 kg load for the bulk hardness of the steels. The cross-sectional microhardness profiles were determined using Matsuzawa

microhardness tester with a load of 10 g. The measurements started at a distance of 10 μm from the damaged surface of the steels and continued first in steps of 10 μm up to 40 μm. After that, the measurements were continued in 15 μm steps up to 100, and thereafter at 25–35 μm steps until reaching the bulk material. Each reading is an average of three measurements conducted at the same distance from the wear surface, and 50 μm apart from each other.

The XRD studies were performed using Panalytical Empyrean X-Ray Diffractometer. In the current test set-up, monochromatic Co-K_α radiation at 40 kV and 45 mA was used in the line focus mode. The 2θ range was 20 – 130 °, with 0.013 ° step size at 80 seconds measurement time per step. The unworn samples were finely polished with P2000 roughness SiC paper, while no polishing was conducted on the worn specimens. The volume percentage of retained austenite (RA) was determined using the four peak method described in the standard SP-453 [53], using the peaks of (111), (200), (220), and (311) of austenite.

3. Results

3.1. Characterization of microstructures

Fig. 3a represents a secondary electron micrograph of autotempered martensite with finely distributed carbides. No traces of retained austenite were observed. The lath size of the martensite appears to be relatively short due to the reduced prior austenitic grain size (PAGS), recorded to be 20 μm [8]. The lower bainitic (Fig. 3b) morphology consists of bainitic laths with nano-scaled interlath cementite particles. Similar to the martensitic microstructure, there is no trace of retained austenite in lower bainite. The XRD diffraction patterns in Fig. 4 confirm the above interpretations of the SEM images.

The TRIP steel micrograph (Fig. 3c) reveals an interconnected polygonal ferritic matrix with distributed martensitic and retained austenite (RA) islands. Both blocky and film shaped RA were observed. Moreover, the microstructure contains martensite-austenite, i.e. M/A constituents, observed also in the previously studied TRIP assisted steel [54]. M/A constituents can reportedly have different morphologies, i.e. massive, slender, and dot shaped [55]. The micrograph clearly indicates that the studied TRIP steel has both slender and massive M/A constituents. The slender M/A constituents are distributed along the grain boundaries. The behavior of the M/A constituents is governed by the carbon content of the blocky retained austenite [56]. The high aluminum content has significantly reduced the formation of carbides, enhancing the availability of carbon atoms for austenite stabilization. The QP steel (Fig. 3d) contains the same microconstituents as the TRIP steel, including martensite and RA islands in the polygonal ferritic matrix. The martensitic laths appear to be more acicular than in the

TRIP steel and their overall fraction is higher. In addition, the microstructure contains M/A constituents and both blocky and film shaped RA. However, compared to the TRIP steel, a higher occurrence of film shaped RA along the grain boundaries is evident in the QP steel. The M/A constituents in the QP steel are relatively finer and higher in number than in the TRIP steel. The insufficient growth time during the QP processing results in the slender M/A constituents, in contrast to TRIP steel where both slender and massive M/A constituents are evident. The XRD spectra in Fig. 4 illustrate the presence of RA, ~10 % and ~14 % in the TRIP and QP steels, respectively.

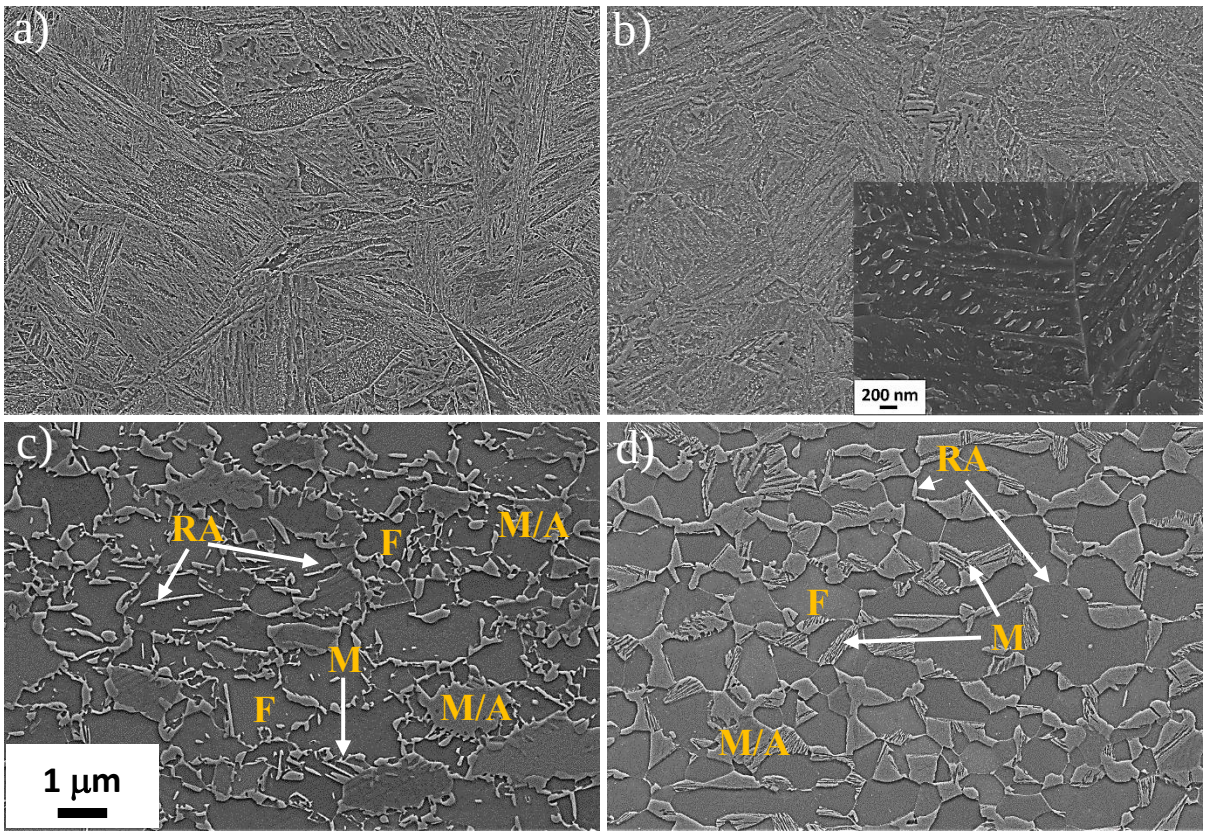

Fig. 3. Microstructures of a) martensite, b) lower bainite, c) TRIP and d) QP steel. RA, M, F and M/A refer to retained austenite, martensite, ferrite, and martensite-austenite constituents, respectively.

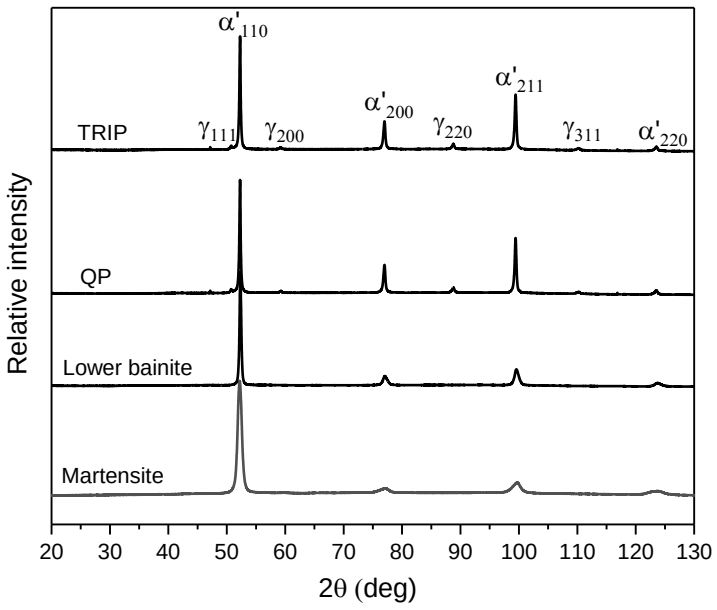

Fig. 4. X-ray diffraction patterns of the steels.

3.2. Wear rates

The wear test results of the steels are shown in Fig. 5 as a function of bulk hardness. The martensitic steel resists wear most efficiently in both tests, followed by lower bainite, QP, and TRIP steel in that order. The CPOD-based ranking exhibits an explicit correlation to the bulk hardness of the steels, revalidating the previous observations [8]. The slurry-pot wear tests, however, demonstrate a slightly different ranking of the steels: the martensitic steel again outperforms all the other steels, but the TRIP steel with the lowest bulk hardness shows performance equal to the QP steel and lower bainite. The results indicate that hardness is not the only factor that determines the wear performance of the steels in the slurry-pot. When the slurry-pot method was compared with the CPOD method, the relative wear performances were observed to be largely influenced by the work hardenability of the steels.

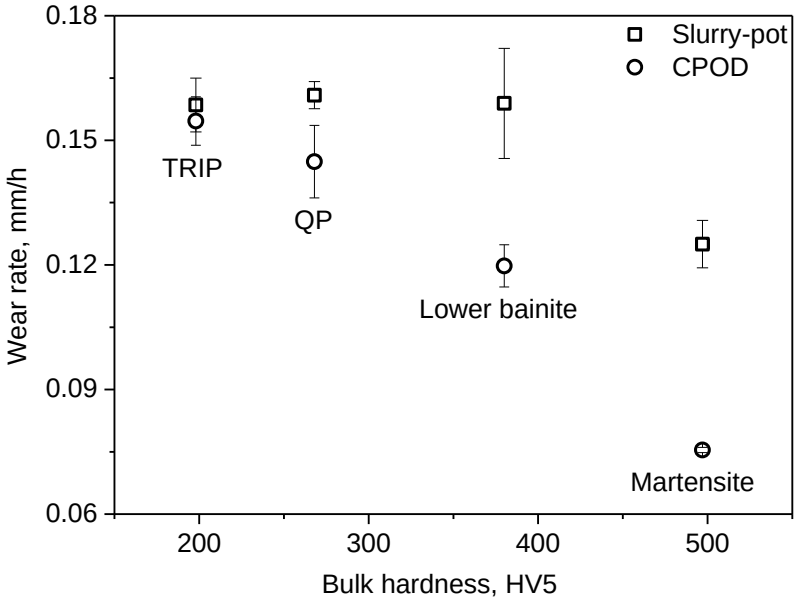

Fig. 5. Comparative wear rates of the steels in the slurry-pot and crushing pin-on-disc (CPOD) tests as a function of bulk hardness (measured using a 5 kg load). Error bars represent the standard error.

3.3. Microhardness profiles

In order to examine the work hardening of the steels, microhardness measurements using a 10 g load were performed from the cross-sections of the wear surfaces towards the matrix. Fig. 6 demonstrates the depth profiles of the steels with a clear increase in the surface hardness after the CPOD and slurry-pot tests. Table 2 shows the maximum hardness, amount of work hardening, and the depth of the work hardened layer for both test methods and all studied steels. The work hardening rate of all steels was higher in the CPOD tests than in the slurry-pot tests. The amount of relative work hardening of the TRIP steel in the CPOD tests was over 150 %, but only 32 % for the martensitic steel. Immediately beneath the wear surface, the CPOD tested martensitic steel exhibits a layer of lower hardness (592 HV, still ~19 % higher than the bulk hardness), approximately ~70 Vickers less than the subsequent maximum hardened layer of 658 HV. Interestingly, the tough plastically deformed layer was characteristically observed smeared over the harder layer in the CPOD tested martensite, explaining the drop and the following increase in the hardness seen in Fig. 6a. For all studied steels, the thickness of the work hardened layer was consistently higher when the tests were conducted with the slurry-pot method.

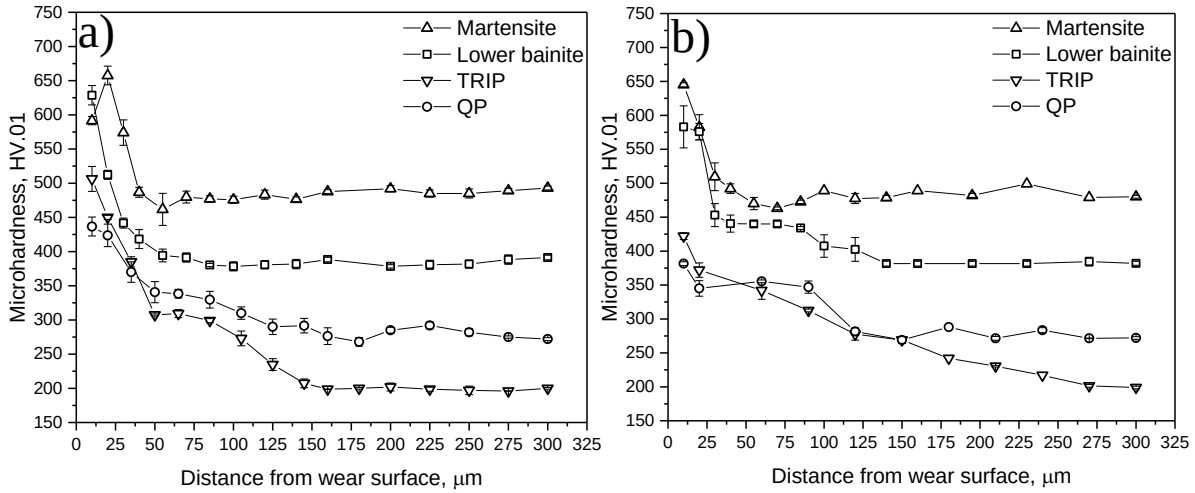

Fig. 6. Microhardness profiles using a 10 g load from the wear surface to the matrix; a) CPOD tests, b) Slurry-pot tests. Error bars represent the standard errors.

Table 2: Surface hardness data of the steels using a 10 g load.

	CPOD			Slurry-pot		
Steels	Surface hardness HV	Work hardening %	Deformation depth μm	Surface hardness HV	Work hardening %	Deformation depth μm
Martensite	658	32	50±10	645	30	70±10
Lower bainite	629	58	50±10	583	47	110±15
QP	437	63	100±10	382	43	110±15
TRIP	506	155	150±15	422	113	250±20

3.4. Wear surface characterization

3.4.1 Optical profilometry

Characterization of the wear surfaces was conducted using optical profilometry and scanning electron microscopy. Fig. 7 presents the color-coded profilometer maps of the wear surfaces for all steels in both test types. The CPOD wear surfaces of the steels are characterized by long groove marks. In contrast, notably shorter grooves and impact marks are evident on the slurry-pot tested wear surfaces.

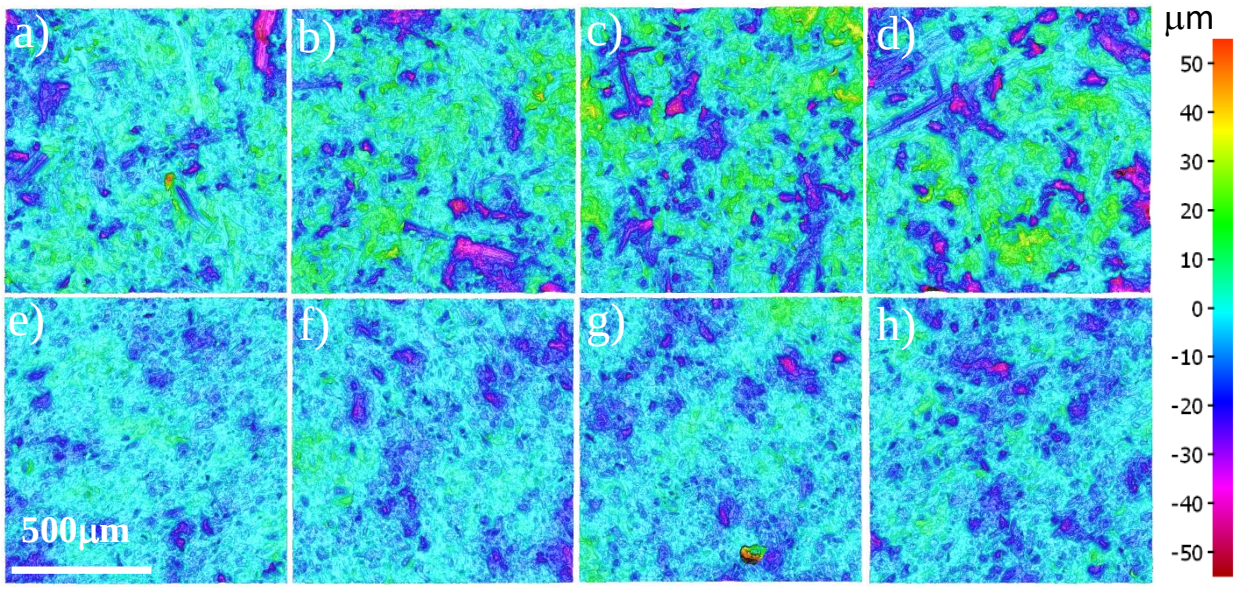

Fig. 7. CPOD wear surfaces: a) martensite, b) lower bainite, c) QP and d) TRIP steel. Slurry-pot wear surfaces: e) martensite, f) lower bainite, g) QP and h) TRIP steel.

The surface roughness parameters also offer indications of the wear behavior of steels [28]. An area of 20×20 mm^2 was selected from each worn steel surface to be scanned with 3D profilometry for the determination of the surface roughness parameters. The root mean square surface roughness (S_q) value provides a more realistic link to the wear response of the material than the commonly used average surface roughness (S_a), as S_q involves the weighted average of an individual sample [28]. Fig. 8a depicts the S_q values of the wear surfaces as a function of the bulk hardness of the steels. The comparison suggests a good agreement between the surface roughness and the wear rates of the steels in the CPOD tests. In contrast, the slurry-pot wear rates are not in accord with the determined roughness values. However, the lowest wear rates of martensite in both wear conditions correspond to the lowest surface roughness of the steel. This is in good agreement with the wear surfaces of the martensitic samples (Fig. 7a and e) exhibiting much shallower damages compared to the TRIP steel samples (Fig. 7d and h).

The wear behavior of the steels in the slurry-pot tests was also evaluated using the impact characterization curves, which have been found to be useful [28] for understanding the impact wear behavior of the steels. Fig. 8b compares the degree of penetration of the steels as a function of bulk hardness, showing that the D_p value of martensite is the lowest and suggesting that its wear rate might also be the lowest. Although the TRIP steel exhibits a comparatively lower wear rate than the QP and lower bainitic steels, its higher value of D_p indicates a high deformation capability of the steel during

the wear process. Lower bainite has a smaller D_p, suggesting that its high initial hardness might have resisted the particle penetration during the impacts. However, the wear performance of the lower bainite was rather poor, indicating that a large fraction of the material displaced from the crater area translated into a wear loss.

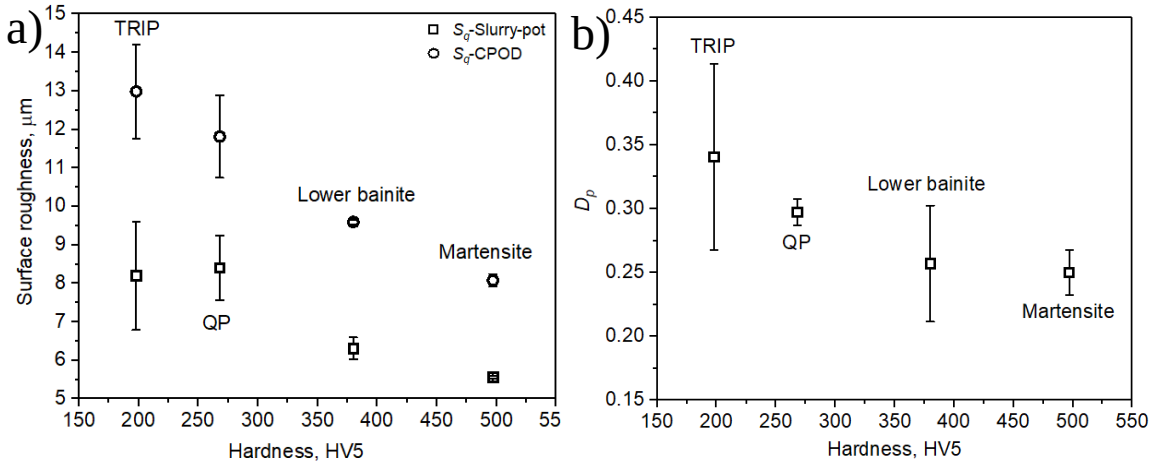

Fig. 8. a) The root mean square surface roughness (S_q) of the steels as a function of bulk hardness, and b) degree of penetration (D_p) of the steels tested in slurry-pot as a function of bulk hardness (load 5 kg). Error bars represent the standard error.

3.4.2 Scanning electron microscopy

The wear surfaces of the steels were characterized by SEM using backscattered electron imaging. In the images, the light grey areas are steel, and the darker areas are embedded rock particles.

The wear surface of martensite tested with CPOD (Fig. 9a) appears smoother than that of the lower bainite (Fig. 9c). The grooves in the lower bainite are comparatively wider and marginally deeper than in the martensite. The grooves in the lower bainite were also associated with surface cracks, contributing to its higher material loss. There were also less embedded granite abrasives in the martensite than in the lower bainite. The shallow grooves combined with the plastic ridges on either side of the grooves in both of these steels, especially in the martensite, indicate a less severe wear mechanism, mainly microploughing. The QP and TRIP steels, in contrast (Fig. 9e and g), underwent more severe grooving due to their lower initial hardness. The deeper grooves along with the minimal presence of adjacent ridges contribute to the material removal mostly by the microcutting wear mechanism. Wedge formation ahead of the grooves is common in the TRIP steel, and during repetitive grooving action by the granite abrasives particles, they become detached from the steel's surface. A similar abrasive entrapment in the surface can also be observed in the TRIP and QP steels.

The craters that are formed by the oblique impacts of the abrasive particles are typical for the slurry-pot tested wear surfaces. The appearance of the craters in all tested steels is rather similar, but in a closer view we can distinguish several important features related to the wear process. As we proceed from martensite through lower bainite to the QP steel (Fig. 9b, d and f), the crater depths and widths increase. In addition, the material accumulation or the wedge formation ahead of the oblique impact point increases in the same order. This observation is fully consistent with the initial hardness and deformation capability of the steels. Although the wedges formed in the martensite were removed quickly by the successive impacts, overall the martensite wear surface appears to contain less surface cracks than the lower bainite and the QP steel. Consequently, martensite is still the best performer among the studied materials in the slurry-pot tests, despite an increase of 40 % in the absolute wear rate compared to CPOD. A general impression of the impact marks on the surface of the TRIP steel (Fig. 9h) is rather uneven with varying depths and widths of the craters, resulting in a relatively large scatter in the D_p values. The abrasive entrapment took place much deeper in the TRIP steel than in the other test materials. As a characteristic feature, plenty of loose material and plastic ridges along the short grooves were adhered to the wear surfaces of the TRIP steel.

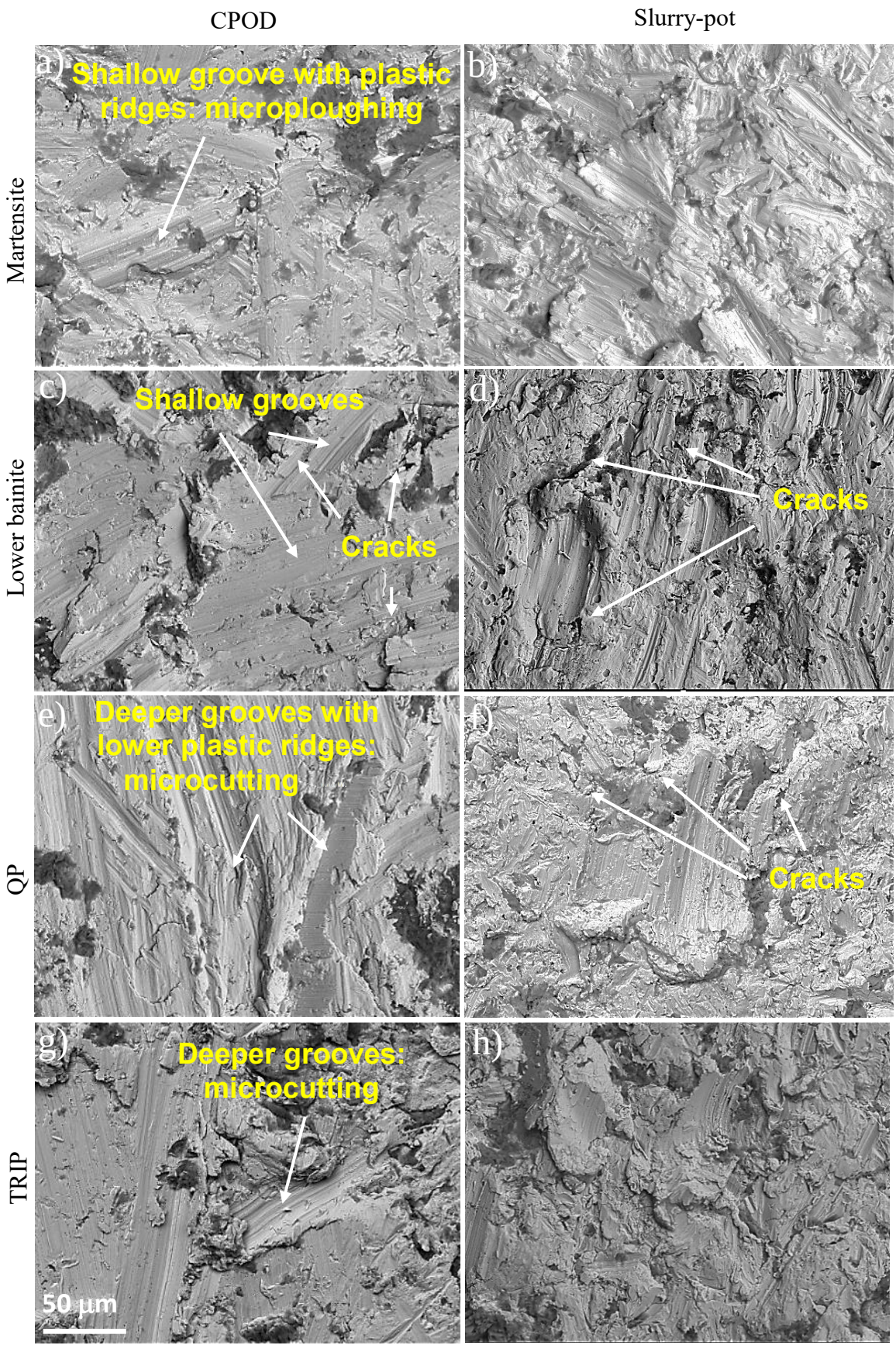
CPOD
Slurry-pot
Martensite
Lower bainite
QP
TRIP
a)
Shallow groove with plastic ridges: microploughing
b)
c)
Shallow grooves
Cracks
d)
Cracks
e)
Deeper grooves with lower plastic ridges: microcutting
f)
Cracks
g)
Deeper grooves: microcutting
50 µm
h)

Fig. 9. CPOD wear surfaces, a) martensite, c) lower bainite, e) QP and g) TRIP steel. Slurry-pot wear surfaces, b) martensite, d) lower bainite, f) QP and h) TRIP steel.

3.5. Subsurface characterization

The deformed subsurface micrographs of the steels tested with the CPOD and slurry-pot devices are depicted in Fig. 10. The martensitic steel in Fig. 10a exhibits two types of subsurface deformations in the CPOD tests: the more common one entails brittle surface shear bands with a thickness ranging from 5 to 15 μm, facilitating surface cracks and material removal. In another instance, a plastically deformed layer was observed smeared over the fully transformed shear bands in the opposite direction of the material flow. The plastically deformed layer had lower hardness than the underlying fully transformed layer, consistent with the reduced microhardness values obtained immediately below the wear surface shown in Fig. 6a. Moreover, Fig. 10a points out that the subsurface cracks in the CPOD tested martensite are actually restricted by the deformed plastic material, delaying the crack propagation and subsequent material removal. In the slurry-pot tests, martensite showed surface shear bands similar to CPOD. Additionally, the subsurface ASBs were also more common in the slurry-pot tested martensite in contrast to the CPOD tests, contributing to the increase of the wear rate in the slurry-pot. Fig. 10b represents a subsurface ASB promoting crack initiation and propagation parallel to the wear surface. Moreover, it was observed that the ASBs had different microstructures at different locations depending on the local conditions of loading and heat dissipation.

Figs. 10c and d show the lower bainite subsurface micrographs of the samples tested with the CPOD and slurry-pot devices. Both microstructures reveal severe deformation and alignment of the matrix. However, in the CPOD tests the subsurface cementite particles appear to maintain their shape without observable fracturing, although at the carbide-matrix interface there seems to be some degree of crack formation. In contrast, the slurry-pot tested subsurface clearly contains comminuted carbides, indicating fragmentation. Additionally, a higher degree of cracking at the carbide-matrix interface is evident, leading to an increase in the material removal.

The QP steel also shows alignment of the matrix towards the sliding direction in the CPOD tests (Fig. 10e), while in the slurry-pot tests (Fig. 10f) the matrix has undergone both alignment and compression during the impacts. The CPOD subsurface exhibits deformed and elongated M/A constituents along the wear direction, creating a large number of voids that further assist the wear process. No visible phase transformation was observed in this case. In contrast to this, the M/A constituents in the slurry-pot tests were deformed and strain induced transformation may have occurred, as the martensitic constituents at

the surface in Fig. 10f evidence. The matrix in the slurry-pot samples exhibits fewer voids than the CPOD subsurface, which could possibly be the main contributing factor to this steel's better performance in the slurry-pot test compared to the CPOD test.

The typical wear responses of the TRIP steel are depicted in Figs. 10g and h for the CPOD and slurry-pot tests, respectively. The CPOD subsurface shows long and relatively closed cracks oriented parallel to the worn surface. In contrast, the slurry-pot tested samples commonly show cracks induced by the embedded abrasives perpendicular to the plane of the surface. A distinguishable feature in Figs. 10g and h is the direction of the crack propagation, which in both cases most probably is a factor notably affecting the wear rate. The cracks in the CPOD subsurface can be seen to propagate through the interconnected weak ferritic matrix, which increases the wear rate. In the slurry-pot tests, however, the cracks were observed in most cases to be restricted by the encountered M/A constituents ahead of the crack tips, resulting in a better relative performance.

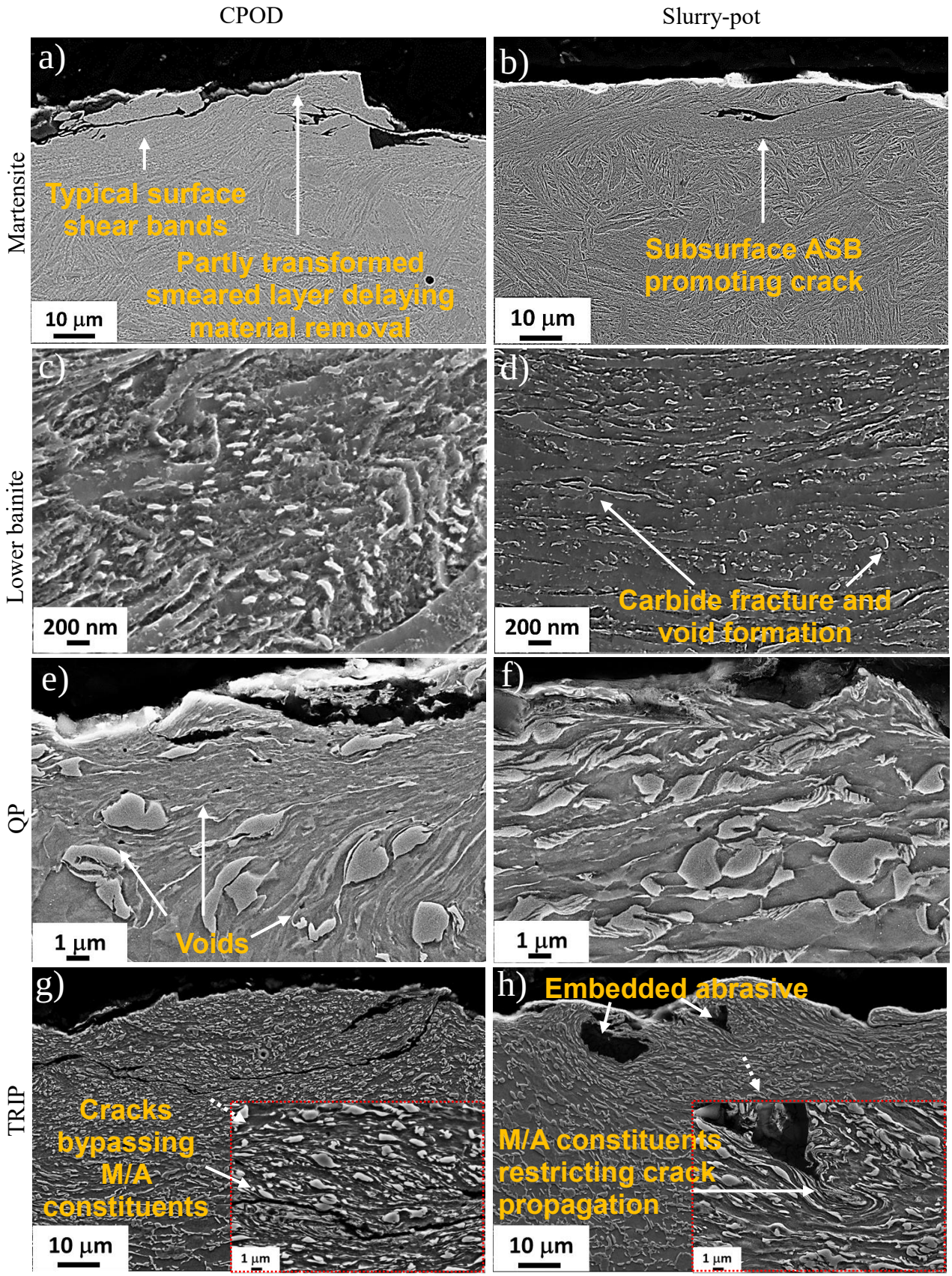

Fig. 10. CPOD subsurfaces of a) martensite, c) lower bainite, e) QP and g) TRIP steel; Slurry-pot

subsurfaces of b) martensite, d) lower bainite, f) QP and h) TRIP steel.

4. Discussion

In this study, four steels were subjected to CPOD and slurry-pot wear tests. The CPOD tests showed a linear correlation between the wear resistance and the bulk hardness of the steels. By contrast, in the slurry pot tests the performance of the QP and bainitic steels was no better than that of the softer TRIP steel, and the magnitude of the benefit offered by the martensitic steel was also somewhat reduced. The change in the relative performance values for the four steels can be attributed to the change in the wear conditions from abrasive to impact-abrasive [8]. In this study, it was seen that the slurry-pot's impact conditions caused an increase in the depth of work hardening, especially for the QP and TRIP steels. The enhanced work hardening of the QP and TRIP steels in the impact-abrasive wear conditions is associated with the transformation of RA to martensite [57,58].

4.1. Wear performance based on hardness-toughness properties

The surface roughness profiles of the steels support the wear performance versus hardness correlation in the CPOD tests. On the other hand, the reduced S_q values of the TRIP steel in the slurry-pot compared to the CPOD tests suggest that the high-angle impingement in the slurry-pot promotes plastic deformation and subsequent ridge formation (microploughing dominant) rather than direct material removal (microcutting dominant) as promoted by the tangential sliding action combined with the high contact force in the CPOD. The generally inverse correlation between the degree of penetration (D_p) and bulk hardness obtained from the slurry-pot tests (Fig. 8b) indicates that the higher depth of penetration in the TRIP steel might not have translated directly into material loss as in the lower bainite. Fig. 11 clearly differentiates the wear performance of the steels in the slurry-pot as a function of the degree of penetration (D_p). In the case of martensite, the lower degree of penetration is quite evidently directly associated with the reduced wear loss. On the other hand, the lower bainite also shows relatively low degree of penetration but similar wear performance as the QP and TRIP steels. This demonstrates that the material displaced from the crater area in lower bainite has directly translated into material loss. In contrast, the material displaced from the craters in the QP and TRIP steels was plastically deformed and showed better adherence, contributing to the similar wear performance as the lower bainite despite the higher degree of penetration. Therefore, a significant amount of energy is spent in the plastic deformation, causing transformation of retained austenite to martensite in the TRIP and QP steels and improving their relative performance compared to the (initially) much harder steels in the slurry-pot conditions.

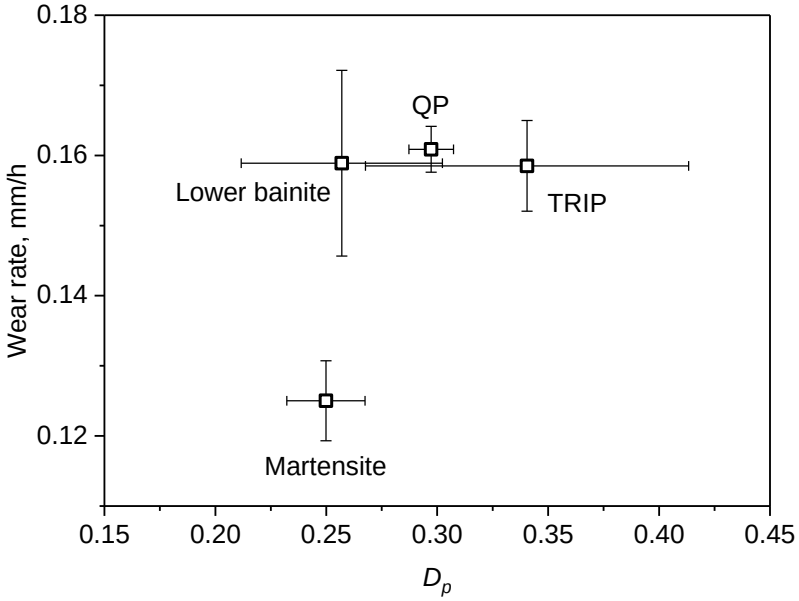

Fig. 11. Wear performance of the steels in the slurry-pot as a function of the degree of penetration (D_p). Error bars represent the standard error.

However, the transformation of retained austenite critically depends on the abrasive loading conditions. For instance, a detrimental effect of retained austenite transformation was reported on the dry sliding wear response of carburized steels, resulting in premature wear due to microcracking [59]. The TRIP and QP steels studied in this work, containing an appreciable amount of retained austenite, were severely damaged by the abrasive action of the granite abrasives during the CPOD tests, possibly leading to similar premature wear as observed in [59]. Nonetheless, the TRIP steel performed quite similar to the QP and lower bainite steels in the slurry-pot tests despite its considerably lower initial hardness, indicating an efficient exploitation of the retained austenite in the impact-abrasive conditions.

Compared to the purely abrasive conditions, the harder steels, i.e., martensite and lower bainite, showed lesser magnitudes of performance benefit in the impact-abrasive conditions, presumably due to their reduced capacity for plastic deformation. In this wear environment, the high impact energies caused the embedment of granite abrasives, promoted subsurface shear band formation, and produced a heavily deformed subsurface tribolayer consisting of pores and cracks, accelerating the material removal [8,60]. On the other hand, in the abrasive conditions the martensitic steels exhibit mostly ploughing type of wear with a lower cutting depth, as the higher hardness offers a higher resistance to penetration [8]. Moreover, the abrasive wear resistance of the quenched and tempered steels correlate well with the abraded surface hardness [58]. In the CPOD tests, the martensitic steel showed ploughing type of wear on the surface and a plastically deformed layer in the subsurface. This suggests that the

surface hardness of the martensitic steel increases the critical degree of penetration for the transition between ploughing and cutting wear modes, which is in agreement with the proposed theory of Hokkirigawa et al. [61]. Therefore, it can be concluded that the CPOD tested martensite showed relatively better wear performance due to its resistance to penetration and the predominantly ploughing type of wear. The combined effect of these two factors is responsible for the reduced volume of removed debris for a given groove volume. On the contrary, the change in the wear condition from abrasion to impact abrasion in the slurry-pot deteriorated the relative performance of martensite by producing a deformed subsurface promoting cracking.

The CPOD tested lower bainite exhibited a surface hardened layer without any underneath flow of material as found in martensite. This indicates that the abraded surface layer in the lower bainite steel loses its toughness, which eventually shows as a higher wear rate compared to martensite. Lindroos et al. [62] observed that steels with the highest surface hardening were not the best wear resistant materials in abrasive conditions. However, the higher initial hardness explains why lower bainite performs better than the TRIP and QP steels in the CPOD abrasive environment. Nonetheless, when subjected to impact-abrasive conditions in the slurry-pot tests, the lower bainite exhibited a similar performance as the TRIP and QP steels. This is in good agreement with the experiments of Rendon et al. [60], where the hardness of steels played the key role in pure abrasive conditions, while toughness influenced more the impact-abrasive response of the materials. This necessitates further understanding of the wear responses of the microstructural constituents to explain the wear behavior of steels.

4.2. Wear performance based on microstructural constituents

The deformed subsurface of the steels reveals the wear behavior more explicitly. In CPOD, martensite showed mainly two types of deformation mechanisms contributing to wear: formation of surface shear bands (e.g. white layers) and plastic deformation. The white layers with a nano-scale homogeneous microstructure have high hardness ranging from 560 to 650 HV, and they are brittle in nature and thus prone to cracking [8]. The severe abrasive conditions in CPOD develop surface cracks that propagate along the brittle bands, merge to one another, and finally lead to the removal of material. Underneath the wear surface, commonly a plastically deformed layer obstructs the material removal by blunting the propagating crack tips. Fig. 12a provides a close-up view of branched cracks formed in the subsurface of the CPOD tested martensitic steel. The micrograph also reveals the local flow of material where branching of the crack has occurred. It is well established that fatigue cracks can generate branching due to overloads [63]. On the other hand, the stress intensity factor associated with branching is reduced compared to a single crack, which may prevent the further crack growth [63]. Rendon and Olsson [60]

concluded that the resistance to abrasive grooving is governed by the plastic deformation capability of the material that reduces the tendency to crack propagation. Compared to CPOD, reduced material flow and elongation of the microstructure in the tangential direction was observed in the slurry-pot subsurface. In many cases the underneath surface showed fully transformed adiabatic shear bands. The hardness of the adiabatic shear bands was found to be in the range of 600 to 770 HV, depending on the extent of transformation. Compared to the CPOD case, the blunting effect was less effective in the slurry-pot subsurface and the cracks propagated more easily (Fig. 12b), increasing the wear rate of martensite. Therefore, in both wear conditions the typical wear mechanism is the formation of a brittle white layer in the surface and its subsequent removal. Nonetheless, the lower wear rate in the CPOD can be attributed to the branching of cracks, whereas the increased wear rate in the slurry-pot is due to the formation of ASBs facilitating single cracks and removal of material in larger chunks.

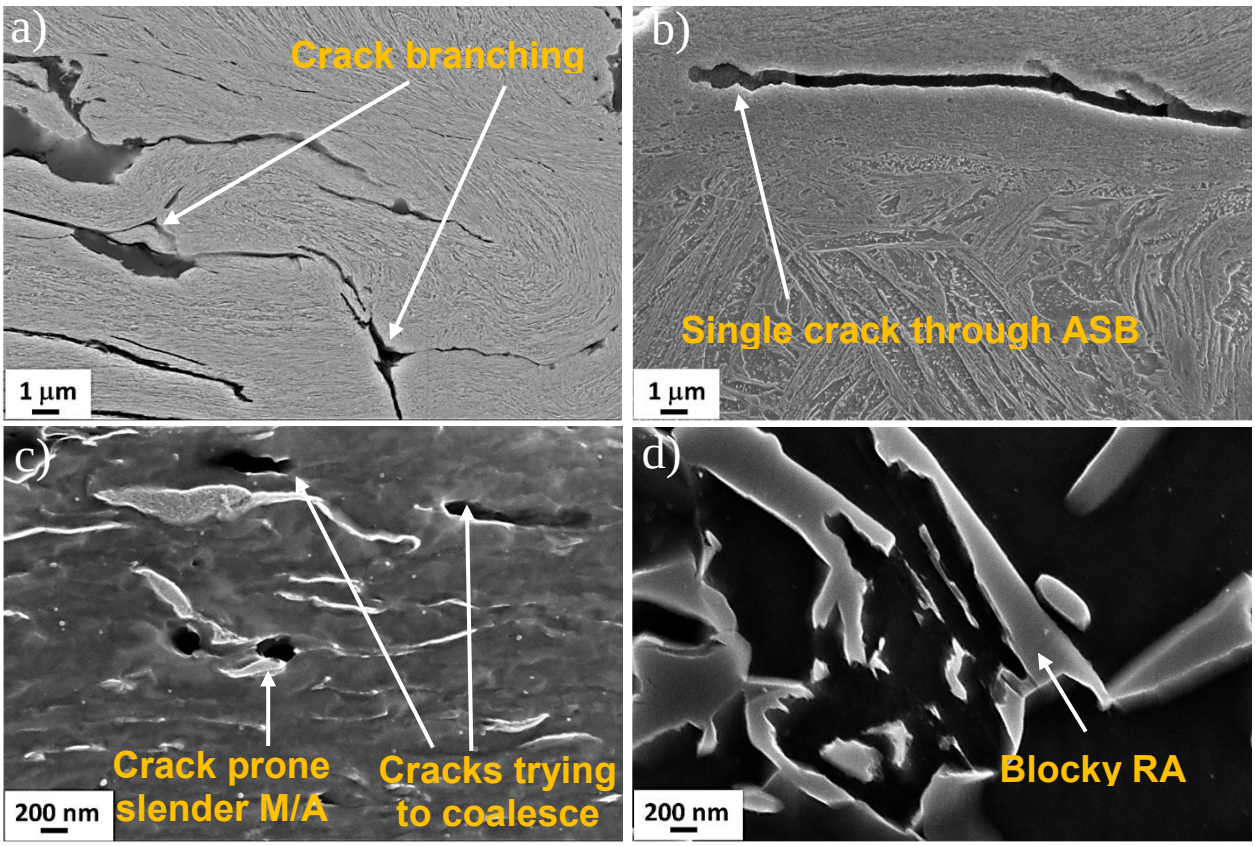

Fig. 12. SEM images of the wear surface cross-sections; a) subsurface crack branching in CPOD tested martensite and b) single crack propagation along an ASB in slurry-pot tested martensite, c) CPOD tested QP steel subsurface, d) blocky retained austenite in the TRIP steel.

The wear behavior of lower bainite is governed by the cracks nucleated at the carbide-matrix interfaces, and to some extent also by the fracturing of the cementite particles. Both favorable [3] and detrimental effects [64] of the cementite particles have been reported in the rolling-sliding abrasion of bainite. Moreover, carbides promoting wear in the impact-abrasive conditions by causing disruption in the plastic flow and leading to high strain gradients and subsequent void formation have also been reported [65]. In the present case, the CPOD tested lower bainite subsurface showed that the cementite particles were aligned towards the wear direction but retained their shapes. Moreover, the carbide-matrix interfaces appear to be stronger, i.e., less prone to cracking. Both of these factors apparently contribute to the improved wear resistance of bainite in the severely abrasive CPOD environment. However, in the impact-abrasive conditions, the carbide-matrix interface shows higher susceptibility to cracking due to the repetitive impacts by the abrasives. Moreover, the cementite particles appear to be slightly more comminuted than those in the CPOD subsurface. The combined effect of these factors seems to have caused fragmentation of carbides and nucleation of cracks at the interfaces between the matrix and the carbides, contributing to the increased wear rate in the slurry-pot environment.

The wear responses of QP and TRIP steels were largely influenced by the retained austenite content and the martensite-austenite constituents and their morphologies. The TRIP assisted steels resisted wear mainly by the transformation of retained austenite to martensite by the load exerted during the wear process. The XRD analysis of the QP steel in Table 3 shows a small amount of RA after the CPOD tests, while no RA was present after the slurry-pot tests. In contrast, no traces of retained austenite were observed in the TRIP steel in either wear tests. The reliable detection limit for contemporary XRD equipment is considered to be 0.5 % [66].

Table 3: Retained austenite (RA) content of QP and TRIP steels before and after the wear tests.

	QP			TRIP		
	Unworn	CPOD	Slurry-pot	Unworn	CPOD	Slurry-pot
% RA	14	2	Trace (> 0.50 %)	10	Trace (> 0.50 %)	Trace (> 0.50 %)

The increased wear surface hardness of the QP steel also supports the formation of stress induced martensite. However, evidently the transformation benefited the QP steel only in the slurry-pot testing while being detrimental in the CPOD tests. Table 3 shows that after the CPOD test, the RA content of QP steel was still 2 %. This indicates that the abrasive wear offered by CPOD was not capable of fully transforming the RA to martensite in the case of the QP steel. This is probably due to the fact that

compared to the TRIP steel, the QP steel contained a higher amount of film shaped RA, which is claimed to be more stable than the blocky RA [67]. The role of RA in the deformation of steels is therefore somewhat controversial and depends largely on the loading conditions [58]. To obtain the full advantage of the RA, its stability must be moderate, as the thin films of RA may not guarantee an effective TRIP effect due to the higher mechanical stability caused by the constraint from the surrounding ferrite plates, reduced potential nucleation sites for martensite [20], and higher carbon content [68]. On the other hand, the lower mechanical stability of RA causes its premature transformation to martensite with a little effect on the work hardening in the course of deformation. It seems likely that the mechanical stability of RA is governed by the combined effect of the RA volume fraction, morphology, and carbon content [66]. Therefore, a plausible wear mechanism for the QP steel in the CPOD test can be outlined in the following manner: Once the CPOD wear process commences, the blocky RA starts to transform to martensite practically right away, i.e., prematurely as regards the positive influence of the TRIP effect on the wear resistance of the steel. As shown by Speer et al. [69], at the temperature of 350 $^{\circ}$C the excess carbon can diffuse away from the transformed martensite very fast (in less than 0.1 s), readily increasing the carbon content of the adjacent film shaped RA in the QP steel. Although the surface temperature of the steels in the CPOD test hardly reach such high temperatures, the diffusion rate of carbon may still become sufficient to provide a similar effect but in a bit longer time scale. The excess carbon provides additional stability to the film shaped RA, hindering its participation in the CPOD wear process. The work of Shen et al. [66] also indicates that local dispersion of microstructures reduces the effective path of diffusion, which in turn favors the diffusion of carbon in the neighboring RA lamellae, increasing their stability. This mechanism was beneficial in the working conditions of Shen et al. [66], but possibly had a detrimental effect in the present case where the film shaped RA became overly stable rendering it ineffective to participate in the CPOD abrasive wear process. Additionally, the incoherency between the primary martensite and the untempered martensite transformed due to plastic deformation reduces the stress accommodation capability of the microstructure, facilitating subsurface cracks [69] during the CPOD test. The CPOD tested QP subsurface (Fig. 10e) had plenty of voids but hardly any signs of transformed martensite underneath the surface, which clearly distinguishes it from the slurry-pot tested subsurface (Fig. 10f). Hence, in the case of the QP steel tested with CPOD, it is possible that the newly formed untempered martensite becomes quickly detached from the matrix due to the subsurface cracks, leading to a higher material removal rate. In contrast, the mechanical stability of the retained austenite in the QP steel was possibly optimal (moderately stable) for the impact-abrasive loading conditions offered by the slurry-pot tester, where the transformation to martensite occurred only gradually, providing additional strength to the ferritic matrix in the course of the impact-abrasive wear process.

Early reports claim that cleavage cracks are sensitive to the morphologies of the M/A constituents [70,71], the slender morphologies being more crack prone than the massive morphologies [72]. A closer view of the CPOD tested QP steel subsurface in Fig. 12c reveals cracked M/A constituents that have aligned in the wear direction. The propagating cracks tend to coalesce with each other through the weak ferritic matrix, resulting in a higher wear rate. In contrast, the slurry-pot deformed subsurface of the QP steel in Fig. 10f clearly shows the higher presence of newly transformed martensite, providing additional support to the matrix.

Although the TRIP steel had the same constituents and only a slightly lower RA content than the QP steel, the damage subsurfaces revealed different responses of the microstructural constituents contributing to wear. The blocky morphology of the retained austenite in the TRIP steel (Fig. 12 d) reduced its mechanical stability, leading to its early transformation to martensite and eventual premature failure of the steel during the CPOD wear process. This also explains the practically zero RA content of the TRIP steel after the CPOD wear tests. However, the abrasive action in the CPOD test hardened the material surface, leading also to the nucleation of cracks at the most severely deformed locations of the microstructure. The typical material removal mechanism from the CPOD tested subsurface of the TRIP steel can be attributed to the propagating cracks through the interconnected ferritic matrix bypassing the M/A constituents. Fig. 10g suggests that with the progression of wear, the cracks propagate parallel to the wear direction through the weak ferritic matrix. It also seems unlikely that the aligned M/A constituents trigger any martensite transformation ahead the crack tip, but rather allow easy passage for the propagating cracks, leading to a higher material removal rate. The critical difference in the deformation of the slurry-pot and CPOD tested TRIP steels is the direction of the cracks: in the slurry pot tests, the cracks nucleated at the contact surface eventually propagated in the direction normal to the wear surface, while in the CPOD tests the crack propagation direction is essentially parallel to the wear surface. Compared to the CPOD tests, the ferritic matrix can also be expected to be stronger in the slurry pot tested samples due to the complete and gradual transformation of the retained austenite to martensite. It is likely that the transformation of RA to martensite ahead of the crack tip quickly retarded the crack propagation. Moreover, as already discussed above, the massive M/A constituents prevalent in the TRIP steel are less prone to cracking than their slenderer counterparts and can therefore also act as barriers to the crack tip advancement. However, it was quite difficult to precisely locate and distinguish the massive M/A constituents in the micrographs due to the significantly deformed subsurface of the TRIP steel. In any case, the impact load was strong enough to transform the RA and the peripheral retained austenite of the M/A constituents into martensite and thus to strengthen

the matrix. Additionally, the blunting effect offered by the M/A constituents reduced the further propagation of the crack tips, improving the wear resistance of the TRIP steel in the impact-abrasive wear conditions.

5. Conclusions

This research work deals with abrasive and impact-abrasive wear behavior of four steels, including a martensitic, lower bainitic, quench and partitioning (QP), and transformation induced plasticity (TRIP) steel. The wear tests were conducted using the crushing pin-on-disc (CPOD) and slurry-pot test methods. The main conclusions of this work can be summarized as follows:

- CPOD wear testing ranks the steels according to their initial hardness. The slurry-pot method, however, is more realistic if the (intended) application involves impacts in addition to pure abrasive conditions.
- Martensite is preferred over lower bainite in both wear conditions. In pure abrasive wear, the ability of martensite to deform plastically improved its wear resistance by the crack blunting mechanism. In the impact-abrasive conditions, the reduced performance benefit of martensite can be attributed to the formation of adiabatic shear bands (ASB's).
- Lower bainite experienced severe wear in the impact-abrasive conditions mainly due to the nucleation of cracks at the carbide-matrix interface.
- In both studied wear conditions, the overall wear performance of the TRIP assisted steels was rather poor compared to the other two studied steels. However, the relative wear performance of the TRIP steels was slightly improved in the impact-abrasive conditions.

Acknowledgements

The authors gratefully acknowledge M.Sc Leo Hyvärinen for his help with the XRD experiments, and Mr. Ari Varttila and Mr. Leevi Kurki for preparing the samples. This work made use of Tampere Microscopy Center facilities at Tampere University.

6. References

[1] R. Devanathan, P. Clayton, Rolling-sliding wear behavior of three bainitic steels, Wear. 151 (1991) 255–267. https://doi.org/10.1016/0043-1648(91)90253-Q.

[2] P.H. Shipway, S.J. Wood, A.H. Dent, The hardness and sliding wear behaviour of a bainitic steel, Wear. 203–204 (1997) 196–205. https://doi.org/10.1016/S0043-1648(96)07411-X.

[3] C. Chattopadhyay, S. Sangal, K. Mondal, A. Garg, Improved wear resistance of medium carbon

microalloyed bainitic steels, Wear. 289 (2012) 168–179. https://doi.org/10.1016/j.wear.2012.03.005.

[4] N. Jin, P. Clayton, Effect of microstructure on rolling/sliding wear of low carbon bainitic steels, Wear. 202 (1997) 202–207. https://doi.org/10.1016/S0043-1648(96)07271-7.

[5] J.E. Garnham, J.H. Beynon, Dry rolling-sliding wear of bainitic and pearlitic steels, Wear. (1992). https://doi.org/10.1016/0043-1648(92)90189-F.

[6] P. Clayton, K.J. Sawley, P.J. Bolton, G.M. Pell, Wear behavior of bainitic steels, Wear. (1987). https://doi.org/10.1016/0043-1648(87)90067-6.

[7] A. Ghaderi, G. Saha, T. Guo, D. Fabijanic, M.R. Barnett, Material wear map for ground-engaging steels based on scratch tests, Wear. 404–405 (2018) 153–165. https://doi.org/10.1016/j.wear.2018.03.017.

[8] K. Valtonen, N. Ojala, O. Haiko, V.T. Kuokkala, Comparison of various high-stress wear conditions and wear performance of martensitic steels, Wear. 426–427 (2019) 3–13. https://doi.org/10.1016/j.wear.2018.12.006.

[9] K. Valtonen, K. Keltamäki, V.T. Kuokkala, High-stress abrasion of wear resistant steels in the cutting edges of loader buckets, Tribol. Int. 119 (2018) 707–720. https://doi.org/10.1016/j.triboint.2017.12.013.

[10] Y.Y. Yang, H.S. Fang, W.G. Huang, A study on wear resistance of the white layer, Tribol. Int. (1996). https://doi.org/10.1016/0301-679X(95)00099-P.

[11] C. Zener, J.H. Hollomon, Effect of strain rate upon plastic flow of steel, J. Appl. Phys. (1944). https://doi.org/10.1063/1.1707363.

[12] Z.Q. Duan, S.X. Li, D.W. Huang, Microstructures and adiabatic shear bands formed by ballistic impact in steels and tungsten alloy, Fatigue Fract. Eng. Mater. Struct. (2003). https://doi.org/10.1046/j.1460-2695.2003.00705.x.

[13] Z.H. Chen, L.C. Chan, T.C. Lee, C.Y. Tang, An investigation on the formation and propagation of shear band in fine-blanking process, in: J. Mater. Process. Technol., 2003. https://doi.org/10.1016/S0924-0136(03)00141-9.

[14] J. Speer, D.K. Matlock, B.C. De Cooman, J.G. Schroth, Carbon partitioning into austenite after martensite transformation, Acta Mater. 51 (2003) 2611–2622. https://doi.org/10.1016/S1359-6454(03)00059-4.

[15] E. Doege, S. Kulp, C. Sunderkötter, Properties and application of TRIP-steel in sheet metal forming, Steel Res. 73 (2002) 303–308.

[16] Y. Tomita, T. Iwamoto, Computational prediction of deformation behavior of TRIP steels under cyclic loading, Int. J. Mech. Sci. 43 (2001) 2017–2034.

[17] X.C. Wei, R.Y. Fu, Dynamic tensile characteristic of high strength low alloy TRIP steel and its modeling., Int, in: Conf. TRIP-Aided High Strength Ferros Alloy., 2002: pp. 287–291.

[18] R.A. Savrai, L.Y. Pychmintsev, Effect of stress state on the transformation behavior and mechanical properties of TRIP-aided automotive steels., Int, in: Conf. TRIP-Aided High Strength Ferros Alloy., 2002: pp. 79–84.

[19] F. Hu, K.M. Wu, P.D. Hodgson, Effect of retained austenite on wear resistance of nanostructured dual phase steels, Mater. Sci. Technol. 32 (2016) 40–48. https://doi.org/10.1179/1743284715Y.0000000061.

[20] C. Garcia-Mateo, F.G. Caballero, T. Sourmail, M. Kuntz, J. Cornide, V. Smanio, R. Elvira, Tensile behaviour of a nanocrystalline bainitic steel containing 3wt% silicon, Mater. Sci. Eng. A. 549 (2012) 185–192. https://doi.org/10.1016/j.msea.2012.04.031.

[21] J.G. Speer, D. V. Edmonds, F.C. Rizzo, D.K. Matlock, Partitioning of carbon from supersaturated plates of ferrite, with application to steel processing and fundamentals of the bainite transformation, Curr. Opin. Solid State Mater. Sci. 8 (2004) 219–237. https://doi.org/10.1016/j.cossms.2004.09.003.

[22] M.J. Santofimia, T. Nguyen-Minh, L. Zhao, R. Petrov, I. Sabirov, J. Sietsma, New low carbon Q&P steels containing film-like intercritical ferrite, Mater. Sci. Eng. A. (2010). https://doi.org/10.1016/j.msea.2010.06.083.

[23] C. Wang, J. Shi, S. Liu, S. Du, H. Dong, Study on three-body impact-abrasion of steel treated by quenching-partitioning-tempering process, Cailiao Yanjiu Xuebao/Chinese J. Mater. Res. 23 (2009) 305–310.

[24] O. Haiko, M. Somani, D. Porter, P. Kantanen, J. Kömi, N. Ojala, V. Heino, Comparison of impact-abrasive wear characteristics and performance of direct quenched (DQ) and direct quenched and partitioned (DQ&P) steels, Wear. 400–401 (2018) 21–30. https://doi.org/10.1016/j.wear.2017.12.016.

[25] J.H. Tylczak, J.A. Hawk, R.D. Wilson, A comparison of laboratory abrasion and field wear results, Wear. 225–229 (1999) 1059–1069. https://doi.org/10.1016/S0043-1648(99)00043-5.

[26] D. Tolfree, Investigation of the Gouging Abrasion Resistance of Materials in the Mining Industry, (2000) 110. https://open.library.ubc.ca/cIRcle/collections/ubctheses/831/items/1.0081124#downloadfiles.

[27] J.A. Hawk, R.D. Wilson, J.H. Tylczak, Ö.N. Doğan, Laboratory abrasive wear tests: Investigation of test methods and alloy correlation, Wear. 225–229 (1999) 1031–1042. https://doi.org/10.1016/S0043-1648(99)00042-3.

[28] Gourab Saha, Abrasive wear of alloys for ground engaging tools, Deakin University, 2017. http://hdl.handle.net/10536/DRO/DU:30103712.

[29] L. Xu, S. Clough, P. Howard, D. Stjohn, Laboratory assessment of the effect of white layers on wear

resistance for digger teeth, Wear. 181–183 (1995) 112–117. https://doi.org/10.1016/0043-1648(94)07001-6.

[30] K. Valtonen, V. Ratia, N. Ojala, V.T. Kuokkala, Comparison of laboratory wear test results with the in-service performance of cutting edges of loader buckets, Wear. 388–389 (2017) 93–100. https://doi.org/10.1016/j.wear.2017.06.005.

[31] B. Zhang, Y. Liu, W. Shen, Y. Wang, X. Tang, X. Wang, A study on the behavior of adiabatic shear bands in impact wear, Wear. 198 (1996) 287–292. https://doi.org/10.1016/0043-1648(96)07209-2.

[32] V. Ratia, K. Valtonen, A. Kemppainen, V.-T. Kuokkala, High-Stress Abrasion and Impact-Abrasion Testing of Wear Resistant Steels, Tribol. Online. 8 (2013) 152–161. https://doi.org/10.2474/trol.8.152.

[33] S.L. Rice, Formation of subsurface zones in impact wear, ASLE Trans. 24 (1981) 264–268. https://doi.org/10.1080/05698198108983020.

[34] M. Lindroos, V. Ratia, M. Apostol, K. Valtonen, A. Laukkanen, W. Molnar, K. Holmberg, V.-T. Kuokkala, The effect of impact conditions on the wear and deformation behavior of wear resistant steels, Wear. 328–329 (2015) 197–205. https://doi.org/http://dx.doi.org/10.1016/j.wear.2015.02.032.

[35] A.K. Cousens, The Erosion of Ductile Metals by Solid Particle Impact, n.d. http://www.repository.cam.ac.uk/handle/1810/244796.

[36] I. V. Kragelsky, A.I. Zolotar, A.O. Sheiwekhman, Theory of material wear by solid particle impact - a review, Tribol. Int. 18 (1985) 3–11. https://doi.org/10.1016/0301-679X(85)90002-7.

[37] M. Kirchgaßner, E. Badisch, F. Franek, Behaviour of iron-based hardfacing alloys under abrasion and impact, Wear. 265 (2008) 772–779. https://doi.org/10.1016/j.wear.2008.01.004.

[38] S.F. Wayne, S.L. Rice, K. Minakawa, H. Nowotny, The role of microstructure in the wear of selected steels, Wear. 85 (1983) 93–106. https://doi.org/10.1016/0043-1648(83)90338-1.

[39] J.F. Archard, W. Hirst, The wear of metals under unlubricated conditions, in: Proc. R. Soc. London. Ser. A. Math. Phys. Sci., The Royal Society, 1956: pp. 397–410. https://doi.org/10.1098/rspa.1956.0144.

[40] K.A. Koji Kato, Wear mechanisms, Lubr. Reliab. Handb. (2007) 1–3. https://doi.org/10.1016/b978-075065154-7/50113-3.

[41] D.A. Rigney, L.H. Chen, M.G.S. Naylor, A.R. Rosenfield, Wear processes in sliding systems, Wear. 100 (1984) 195–219. https://doi.org/10.1016/0043-1648(84)90013-9.

[42] K. Kato, Abrasive wear of metals, Tribol. Int. 30 (1997) 333–338. https://doi.org/10.1016/S0301-679X(96)00063-1.

[43] N. P. Suh, The delamination theory of wear, Wear. 25 (1973) 111–124.

https://doi.org/http://dx.doi.org/10.1016/0043-1648(73)90125-7.

[44] J. Terva, T. Teeri, V.T. Kuokkala, P. Siitonen, J. Liimatainen, Abrasive wear of steel against gravel with different rock-steel combinations, Wear. 267 (2009) 1821–1831. https://doi.org/10.1016/j.wear.2009.02.019.

[45] R.D. Wilson, J.A. Hawk, Impeller wear impact-abrasive wear test, Wear. 225–229 (1999) 1248–1257. https://doi.org/10.1016/S0043-1648(99)00046-0.

[46] N. Ojala, K. Valtonen, P. Kivikytö-Reponen, P. Vuorinen, V.-T. Kuokkala, High speed slurry-pot erosion wear testing with large abrasive particles, Finnish J. Tribol. 33 (2015) 36–44. https://journal.fi/tribologia/article/view/69243.

[47] N. Ojala, K. Valtonen, A. Antikainen, A. Kemppainen, J. Minkkinen, O. Oja, V.T. Kuokkala, Wear performance of quenched wear resistant steels in abrasive slurry erosion, Wear. (2016). https://doi.org/10.1016/j.wear.2016.02.019.

[48] K. Valtonen, V. Ratia, N. Ojala, V.T. Kuokkala, Comparison of laboratory wear test results with the in-service performance of cutting edges of loader buckets, Wear. 388–389 (2017) 93–100. https://doi.org/10.1016/j.wear.2017.06.005.

[49] V. Heino, K. Valtonen, P. Kivikytö-Reponen, P. Siitonen, V.T. Kuokkala, Characterization of the effects of embedded quartz layer on wear rates in abrasive wear, Wear. 308 (2013) 174–179. https://doi.org/10.1016/j.wear.2013.06.019.

[50] N. Saunders, Z. Guo, X. Li, A.P. Miodownik, J.P. Schillé, Using JMatPro to model materials properties and behavior, Jom. 55 (2003) 60–65. https://doi.org/10.1007/s11837-003-0013-2.

[51] T.N. Minh, Quenching and Partitioning of low alloyed steels, Tampere University of Technology. Publication; Vol. 1451, 2008. https://doi.org/10.1007/s13244-010-0061-4.

[52] K. Hokkirigawa, K. Kato, An experimental and theoretical investigation of ploughing, cutting and wedge formation during abrasive wear, Tribol. Int. 21 (1988) 51–57. https://doi.org/10.1016/0301-679X(88)90128-4.

[53] C.F. Jatczak, Retained Austenite and Its Measurement by X-Ray Diffraction, SAE Tech. Pap. Ser. 1 (2010) 1657–1676. https://doi.org/10.4271/800426.

[54] J. Liu, Z. Zhang, K.I. Manabe, Y. Li, R.D.K. Misra, Microstructure evolution in TRIP-aided seamless steel tube during T-shape hydroforming process, Mater. Charact. (2014). https://doi.org/10.1016/j.matchar.2014.05.020.

[55] I. Kim, H. Nam, M. Lee, D. Nam, Y. Park, N. Kang, Effect of martensite–austenite constituent on low-temperature toughness in YS 500 MPa grade steel welds, Metals (Basel). (2018).

https://doi.org/10.3390/met8080638.

[56] V.G. Haugen, B.R.S. Rogne, O.M. Akselsen, C. Thaulow, E. Østby, Local mechanical properties of intercritically reheated coarse grained heat affected zone in low alloy steel, Mater. Des. (2014). https://doi.org/10.1016/j.matdes.2014.02.010.

[57] B. Liu, W. Li, X. Lu, X. Jia, X. Jin, The effect of retained austenite stability on impact-abrasion wear resistance in carbide-free bainitic steels, Wear. (2019). https://doi.org/10.1016/j.wear.2019.02.032.

[58] A.R. Chintha, Metallurgical aspects of steels designed to resist abrasion, and impact-abrasion wear, Mater. Sci. Technol. (United Kingdom). 35 (2019) 1133–1148. https://doi.org/10.1080/02670836.2019.1615669.

[59] H.J. Kim, Y.G. Kweon, The effects of retained austenite on dry sliding wear behavior of carburized steels, Wear. (1996). https://doi.org/10.1016/0043-1648(95)06634-9.

[60] J. Rendón, M. Olsson, Abrasive wear resistance of some commercial abrasion resistant steels evaluated by laboratory test methods, Wear. 267 (2009) 2055–2061. https://doi.org/10.1016/j.wear.2009.08.005.

[61] K. Hokkirigawa, K. Kato, Z.Z. Li, The effect of hardness on the transition of the abrasive wear mechanism of steels, Wear. 123 (1988) 241–251. https://doi.org/10.1016/0043-1648(88)90102-0.

[62] M. Lindroos, K. Valtonen, A. Kemppainen, A. Laukkanen, K. Holmberg, V.T. Kuokkala, Wear behavior and work hardening of high strength steels in high stress abrasion, Wear. 322–323 (2015) 32–40. https://doi.org/10.1016/j.wear.2014.10.018.

[63] M.A. Meggiolaro, A.C.O. Miranda, J.T.P. Castro, L.F. Martha, Crack retardation equations for the propagation of branched fatigue cracks, in: Int. J. Fatigue, 2005. https://doi.org/10.1016/j.ijfatigue.2005.07.016.

[64] P.W. Hetherington, E.S. Zabawski, Lubricant application, in: K.-H. Grote, E.K. Antonsson (Eds.), Handb. Lubr. Tribol. Vol. II Theory Des. Second Ed., Springer Berlin Heidelberg, 2012: pp. 27-1-27–11. https://doi.org/10.1201/b12265.

[65] A. Ninham, The effect of mechanical properties on erosion, Wear. (1988). https://doi.org/10.1016/0043-1648(88)90208-6.

[66] Y.F. Shen, L.N. Qiu, X. Sun, L. Zuo, P.K. Liaw, D. Raabe, Effects of retained austenite volume fraction, morphology, and carbon content on strength and ductility of nanostructured TRIP-assisted steels, Mater. Sci. Eng. A. 636 (2015) 551–564. https://doi.org/10.1016/j.msea.2015.04.030.

[67] M. Takahashi, H.K.D.H. Bhadeshia, Model for the microstructure of some advanced bainitic steels, Mater. Trans. JIM. 32 (1991) 689–696. https://doi.org/10.2320/matertrans1989.32.689.

[68] H. Bhadeshia, D. V Edmonds, The bainite transformation in a silicon steel, Metall. Trans. A. 10 (1979)

895–907.

[69] D. De Knijf, R. Petrov, C. Föjer, L.A.I. Kestens, Effect of fresh martensite on the stability of retained austenite in quenching and partitioning steel, Mater. Sci. Eng. A. (2014). https://doi.org/10.1016/j.msea.2014.07.054.

[70] A. Lambert-Perlade, A.F. Gourgues, J. Besson, T. Sturel, A. Pineau, Mechanisms and modeling of cleavage fracture in simulated heat-affected zone microstructures of a high-strength low alloy steel, Metall. Mater. Trans. A Phys. Metall. Mater. Sci. 35 (2004) 1039–1053. https://doi.org/10.1007/s11661-004-1007-6.

[71] C.L. Davis, J.E. King, Cleavage initiation in the intercritically reheated coarse-grained heat-affected zone: Part I. Fractographic evidence, Metall. Mater. Trans. A. (1994). https://doi.org/10.1007/BF02651598.

[72] X.J. Di, X. An, F.J. Cheng, D.P. Wang, X.J. Guo, Z.K. Xue, Effect of martensite–austenite constituent on toughness of simulated inter-critically reheated coarse-grained heat-affected zone in X70 pipeline steel, Sci. Technol. Weld. Join. (2016). https://doi.org/10.1080/13621718.2015.1118814.